Available online at www.sciencedirect.com

ScienceDirect

journal homepage: www.elsevier.com/locate/he

Composite anion exchange membranes based on quaternized cardo-poly(etherketone) and quaternized inorganic fillers for vanadium redox flow battery applications

*Sukhwan Yun, Javier Parrondo, Vijay Ramani**

Center for Electrochemical Science and Engineering, Department of Chemical and Biological Engineering, Illinois Institute of Technology, 10 W. 33rd St., Chicago, IL 60616, USA

ARTICLE INFO

Article history:
Received 2 February 2016
Received in revised form
7 April 2016
Accepted 9 April 2016
Available online 13 May 2016

Keywords:
Vanadium redox flow battery
Anion exchange membranes
Organic–inorganic composite membrane
Membrane separator

ABSTRACT

Functionalized organic/inorganic composite anion exchange membranes (AEMs) were prepared with quaternized cardo-poly(etherketone) (QPEK-C) and N-(trimethoxysilylpropyl)-N,N,N-trimethylammonium chloride (TMSP-TMA$^+$Cl$^-$). With an optimized loading of 20wt% of TMSP-TMA$^+$, the sulfate ion conductivity and VO^{2+} permeability of the composite membrane were 8.4 ± 0.2 mScm^{-1} and 0.53 × 10^{-9}cm^{2}s^{-1}, respectively; pristine QPEK-C AEMs had a sulfate ion conductivity of 4.5 ± 0.5 mS cm^{-1} and a VO^{2+} permeability of 1.1 × 10^{-9}cm^{2}s^{-1}. Membranes with 10–20%wt% of TMSP-TMA$^+$ exhibited better mechanical properties, with an ultimate tensile strength of 26 ± 2 MPa and an elongation at break of 32 ± 3%. The chemical and mechanical stabilities of QPEK-C/TMSP-TMA$^+$ composite AEMs were investigated by immersing the membranes in a VO_2^+ solution at 30 °C and monitoring the sulfate ion conductivity and any changes in chemical structure using 1D and 2D-NMR spectroscopy. Nafion® 212, pristine QPEK-C AEM, and QPEK-C/20wt%TMSP-TMA$^+$ composite AEMs were used as separators in an all-vanadium redox flow battery (VRFB). The coulombic efficiencies (CE) (at 100 mAcm^{-2}) were 99% for QPEK-C and QPEK-C/20wt%TMSP-TMA$^+$ and 95% for Nafion® 212. The battery capacity was lowered by 10% over 30 charge–discharge cycles (~60 h) for QPEK-C and QPEK-C/20wt%TMSP-TMA$^+$AEMs. Under similar conditions a loss of 30% of the capacity was observed for the Nafion® 212 separator.

Introduction

During the last decade, green and renewable energy sources such as solar and wind have become highly desirable, increasing the demand for more reliable and efficient electric energy storage systems. The all-vanadium redox flow battery (VRFB) is one of the most promising energy storage systems that is suitable for large-scale applications [1,2]. The VRFB was first proposed and demonstrated in pilot scales by Skyllas-Kazacos et al. [3–10]. Commercial VRFB systems have been manufactured by a number of companies including UniEnergy Technologies and Ashlawn Energy in the United States and Prudent Energy in China [5–8]. The electrolyte solutions in a

* *Corresponding author.*
E-mail address: ramani@iit.edu (V. Ramani).
http://dx.doi.org/10.1016/j.ijhydene.2016.04.060

VRFB contain four different oxidation states of vanadium (V^{2+}, V^{3+}, V^{4+}, and V^{5+}). These solutions are circulated through the positive (V^{4+} and V^{5+}) and negative (V^{2+} and V^{3+}) electrodes during the reversible charge–discharge process [9]. The cross-contamination due to the intermixing of the different redox couples does not result in irreversible damage of the VRFB system. This provides for a battery system with high energy efficiencies (EE) and long lifetime [4].

Cation exchange membranes (CEM) are typically used as solid electrolyte separators in VRFBs, and they are a key component that significantly influence the various efficiency metrics. The properties desired for the CEMs include high ionic conductivity, high selectivity (low permeability towards active elements), reasonable chemical, mechanical and thermal stabilities, and low cost [3,11–13]. Commercial CEMs such as Nafion® (DuPont) [14], Selemion® CMV and AMV (Asahi Glass, Japan) [15], Gore-Select® (W. L. Gore & Associates, Inc.) [16] and Neosepta® (Astom Corp., Japan) [17,18] all exhibit excellent properties. However, they are relatively expensive and this is an obstacle for their wide utilization as separators in VRFBs [19]. Hydrocarbon-based polymer backbones containing aromatic rings have been studied as an alternative to the commercial (perfluorinated) CEMs because of their lower cost and similar properties [13,20–25].

Anion exchange membranes (AEMs) have fixed cationic groups attached to the polymer backbone and are effective in excluding cations present as the active species in the positive and negative electrolytes. For this reason, when employed in VRFBs, they usually result in higher coulombic efficiencies (CE) than CEMs. Positively charged ions can be repelled by the quaternary ammonium groups in AEMs (Donnan exclusion effect) [26], and the narrower hydrophilic channel encountered in aromatic-hydrocarbon-based AEMs typically results in cation permeabilities lower than those observed in perfluorinated CEMs [23,27]. The polymer backbones that have been used as CEMs and AEMs for applications in VRFBs include: poly(arylene ether) [20], poly(fluorenyl ether) [27], poly(ether ether ketone) [28], poly(ether sulfone) [29], polysulfone [22,30], poly(phthalazinone ether ketone) [31], poly(phthalazinone ether ketone ketone) [32], poly(tetramethydi phenyl ether ether ketone) [25], and cardo-poly(ether ketone) (PEK-C) [33]. Several efforts have been made to achieve the desired properties by employing: (a) copolymers, and (b) organic/inorganic composite membranes [4,13,34–36].

Copolymerization of two or more different monomer units permits excellent control of the polymer microstructure, and allows the tuning of transport properties. Kumar et al. prepared AEMs based on poly(vinyl alcohol) (PVA) and copolymers of poly(acrylonitrile-dimethylamino ehtylmethacrylate) (PAN-DMAEMA) [37]. They found that when the DMAEMA concentration increased (from 40 to 70%) in the polymeric membranes, the ion exchange capacity (IEC) increased from 0.78 to 1.18 meq g^{-1}, and that the resulting AEMs performed better in an electrodialysis cell (coulombic efficiency, CE, increased from 80 to 93%). Takimoto et al. synthesized a series of multiblock copolymers with disulfonated poly(arylene ether sulfone) hydrophilic blocks (BPSH) and non-sulfonated poly(arylene ether sulfone) hydrophobic blocks (BPS) and random copolymers with BPSH and BPS [38]. They found that the proton conductivity increased from 76 to 131 mS cm^{-1} when the block length (of the BPSH-BPS block copolymer) increased from 3000 to 10,000 g mol^{-1}. Fang et al. prepared AEMs based on copolymers of N-vinylimidazole and 2,2,2-trifluoroethylmethacrylate and tested them in a VRFB obtaining EEs of 75% at a current density of 50 mA cm^{-2}; Under similar conditions, Nafion® 117 resulted in an EE of 72.6% [34].

When inorganic additives such as silica or titania are incorporated into the polymer matrix, the membrane permeability and the ionic conductivity usually decrease as consequence of presence of fillers in the hydrophobic domains, which reduce the free volume for water uptake, increase channel tortuosity, and distort the ionic channels by affecting how the polymer phases separate at the nanoscale [21,39,40]. Functionalized inorganic additives are highly desirable materials to minimize the negative effect of inorganic fillers on the ionic conductivity. The presence of inorganic fillers with ionic groups anchored to the surface (sulfonic acid, ammonium cations, etc…) helps to retain the ionic conductivity while reducing the permeability by blocking the passage of the species through the ionic channels (the same effect as exhibited by non-functionalized inorganic fillers) [41]. Singh et al. prepared organic/inorganic hybrid AEMs by using 3-aminopropyltriethoxysilane and glycidyltrimethylammonium chloride. The latter two components hydrolyze and condense into a silica network that forms nanoparticles inside the membrane during the fabrication process. The authors were able to improve the ionic conductivity of the composite AEMs by 30% by increasing the additive loading from 50 to 70 wt% [42]. Li et al. prepared organic/inorganic composite AEMs with quaternized poly(arylene ether sulfone) (QPAES) and ZrO_2 filler, and demonstrated that the ZrO_2 crystalline phase facilitated the formation of ionic channels in the hydrated membranes due to the fixed functional groups on the crystalline phase [24]. The hydroxide conductivity increased from 9.5 ± 0.6 mS cm^{-1} for the non-modified polymer to 23.1 ± 2.1 mS cm^{-1} for the composite membrane with 10 wt% ZrO_2. In addition, a 50% improvement in ultimate tensile strength (UTS) (from 25 to 37.5 MPa) was obtained at a 5 wt% ZrO_2 loading. Nagarale et al. prepared poly(vinyl alcohol)/SiO_2 composite AEMs via aqueous dispersion polymerization. When they added 4-vinylpridine (15–35 wt%) to the reaction mixture, the functionalized AEMs exhibited a two-fold increase in the IEC [35]. Wei et al. prepared composite membranes with nanoporous silica combined with poly(vinyl chloride) [34] and poly(tetrafluoroethylene) [43] for use as separators in VRFBs. When employing these composite membrane as separators in a VRFB, their observed EE was approximately 80%, and the battery capacity remained constant over 40 charge–discharge cycles. For a VRFB with Nafion® 115 as the separator, the capacity decreased by 40–50% after 40 charge–discharge cycles.

As shown in the above studies, the polymer backbone and the AEM preparation methods play a significant role in the properties of the membranes. In this study, we have synthesized composite AEMs using quaternized silsesquioxane additives and quaternized cardo-poly(ether ketone) (PEK-C). We aim to improve the ionic conductivity and reduce the vanadium permeability, while maintaining chemical, mechanical, and thermal stability of pristine quaternized PEK-C. The composite membranes were characterized systematically by

chemical, mechanical, and thermal analysis. Charge-discharge cycling in VRFBs using composite AEMs as separators was also performed.

Experimental methods

Synthesis of quaternized PEK-C-based AEMs and preparation of composite AEMs with quaternized PEK-C and quaternized silsesquioxane inorganic additives

Initially, 10 g of PEK-C (Xuzhou Vat Chemical Company, Mn ≈ 38,500 and Mw ≈ 90,700) was dissolved in 500 mL of 1,1,2,2-tetrachloroethane (>98%, Sigma Aldrich). After the polymer was completely dissolved, 6 g of paraformaldehyde (96%, Acros), 25 mL of chlorotrimethylsilane (98%, Acros) and 0.47 mL of tin tetrachloride (>99%, Sigma Aldrich) were added to the reaction mixture. The reaction was carried out at 80 °C and 350 rpm for 240 h. The chloromethylation was stopped by precipitating the chloromethylated PEK-C in 1 L of methanol. The precipitate was recovered by centrifugation (Thermo Scientific, Multifuge X1) at 7500 rpm for 12 min, and purified by re-dissolution in chloroform (anhydrous, >99%, Sigma Aldrich) followed by re-precipitation in methanol. Finally, the purified chloromethylated PEK-C was dried in a vacuum oven at 40 °C for 48 h.

Quaternized PEK-C based AEMs (QPEK-C) were obtained by reacting the chloromethylated PEK-C with trimethylamine. The quaternization reaction was carried out at 30 °C in dimethyl sulfoxide (>99.9%, Sigma Aldrich) [29]. Thin film membranes (with thickness in the range of 45–55 μm) were obtained by casting the previous solution onto glass plates (7.5 cm × 7.5 cm) in a leveled oven at 70 °C for 12 h, followed by heating to 90 °C for 2 h to allow complete evaporation of the solvent.

Organic/inorganic composite AEMs were prepared by addition of N-(trimethoxysilylpropyl)-N,N,N-trimethylammonium chloride (TMSP-TMA$^+$ Cl$^-$) (Gelest, Inc.) to QPEK-C dissolved in dimethyl sulfoxide. Hydrolysis of the TMSP-TMA$^+$ Cl$^-$ precursor during the synthesis resulted in the generation of inorganic nanoparticles. Composite AEMs with 10, 20, 30, and 40 wt% of TMSP-TMA$^+$ Cl$^-$ were prepared. The organic and inorganic components were mixed and stirred for 2 h before casting the suspension in a glass plate (using the same casting procedure described above for pristine QPEK-C AEMs). Pristine QPEK-C AEM and composite AEMs (QPEK-C/TMSP-TMA$^+$) were immersed in 1 M Na_2SO_4 for 24 h to exchange them to the sulfate counter-ion form. Finally, the AEMs were rinsed with deionized water to remove any excess ions adsorbed on the surface, and stored in deionized water until use.

Determination of ion exchange capacity (IEC)

The *IEC* of the AEMs was determined using the Volhard titration method. AEM samples (in the chloride form) of approximately 0.1 g were dried in a vacuum oven at 60 °C for 24 h, weighed to record the dry weight, and immersed in 20 mL of 1 M $NaNO_3$ for another 48 h to ion exchange the chloride initially present. Then, 5 mL of 0.1 N $AgNO_3$ and 3 drops of 0.1 M $Fe(NO_3)_3$ (indicator used to detect the end-point) were added under stirring. The solution was back-titrated using 0.1 N KSCN. The *IEC* was calculated by using the following equation:

$$IEC = 0.1 \times \frac{V_{blank} - V_{eq}}{m} \quad (1)$$

where V_{blank} and V_{eq} are the volume of 0.1 M KSCN employed to reach the equivalence point (mL) for the blank (sample containing 1 M $NaNO_3$ but no AEM) and for the sample; and m is the dry weight of the membrane (g).

Water and 3 M H_2SO_4 solution uptake

Water and sulfuric acid (3 M H_2SO_4) uptake were measured by immersing the AEM samples in the respective media at 30 °C for 24 h. Then, samples were taken from the temperature-controlled oven, liquid drops from the surface were removed, and the weight was quickly recorded to avoid membrane dry out. The samples were then dried in a vacuum oven at 60 °C for 24 h and weighed to determine the dry weight. The following equation was used to determine the water or sulfuric acid uptake (in liquid phase):

$$WU(wt\%) = \frac{W_{hydrated} - W_{dry}}{W_{dry}} \times 100\% \quad (2)$$

where *WU* is the water or sulfuric acid uptake (in weight percentage; wt%), $W_{hydrated}$ is the weight of the samples after equilibration in deionized water or 3 M H_2SO_4 solution, and W_{dry} is the AEM dry weight.

Membrane ionic conductivity

The ionic conductivity of QPEK-C and of the composite membranes (in sulfate form) was measured in a four-electrode conductivity cell. A membrane sample (with an approximate size of 1 cm × 3 cm) was assembled in the four-electrode conductivity cell and immersed in deionized water in a thermostatic bath. Electrochemical impedance spectroscopy (EIS) was used to measure the impedance in the frequency range from 100 kHz to 0.1 Hz (using a Gamry potentiostat; series G750). The high frequency resistance (R_{hf}, Ohm), together with the distance between the electrodes (L, cm), and the membrane thickness (t, cm) and width (w, cm) were used to calculate the membrane ionic conductivity (σ, S/cm) as follows:

$$\sigma = L/(R_{hf} \times t \times w) \quad (3)$$

The dimensions of the membrane (thickness, t; and width, w) were measured for the membrane when fully hydrated.

VO^{2+} ion permeability

To measure the vanadium permeability, the membrane was placed between two compartments of a diffusion cell (20 mL diffusion cell from PermeGear Inc, with an effective area of 4.91 cm^2). The top compartment was filled with 5 mL of 1.5 M $VOSO_4$ in 3 M H_2SO_4 and the bottom compartment was filled with 20 mL of 1.5 M Na_2SO_4 in 3 M H_2SO_4. Samples from the diluted side (Na_2SO_4 solution) were withdrawn at

predetermined time intervals, and the absorbance measured at a wavelength of 745 nm. The concentration of VO^{2+} was estimated using a previously obtained calibration curve. VO^{2+} permeability was determined using the following equation:

$$P = \frac{V_B \times d}{C_A \times A} \times \frac{dC_B}{dt} \quad (4)$$

where P is the membrane permeability to vanadium (IV) ($cm^2\ s^{-1}$), V_B is the volume of solution in the diluted side (20 mL), d is the thickness of the membrane (cm), C_A is the concentration of VO_2SO_4 in the concentrated side (0.5 mol L^{-1}), A is the effective area of membrane exposed to the solutions (4.91 cm^2), and dC_B/dt is the change of the concentration with time (mol L^{-1}; calculated from the measured VO^{2+} concentrations).

Mechanical testing: tensile test

Dynamic mechanical analysis (DMA) was performed to determine the ultimate tensile strength (UTS), elongation at break (EB), and Young's modulus of the AEMs with different TMSP-TMA^+ additive loadings. A Q800 differential mechanical analyzer (TA Instruments) equipped with a relative humidity chamber (DMA-RH Accessory, TA Instruments) and a film tension clamp (TA Instruments) were used in the experiments. The membrane (approximate dimensions: 30 mm × 5 mm × 0.05 mm) was fixed in the film tension clamp using a torque of 9 $lb_F \times$ in., and was then heated to 60 °C under 50% RH. The membrane was allowed to equilibrate for 60 min before starting the test. The tensile test was performed by stretching the membrane at 0.5 MPa min^{-1} until failure.

Thermogravimetric analysis (TGA)

The experiment was performed in a Discovery TGA series thermogravimetric analyzer (TA Instruments) using a high-resolution scan program at 50 °C/min (this program is approximately equivalent to a constant scan rate program at 10 °C/min, but it adjusts the scan rate depending on the rate of weight loss and hence is faster). The experiments were performed while purging the furnace with nitrogen gas (50 mL/min).

Oxidative stability of the composite AEMs in vanadium (V) solution

AEM *ex-situ* oxidative stability was evaluated by immersing QPEK-C/TMSP-TMA^+ composite membranes in 1.5 M $(VO_2)_2SO_4$ + 3 M H_2SO_4 at 30 °C. The ionic conductivity, ultimate tensile stress, elongation at break, and Young's modulus were measured after 24, 72, 168, and 336 h, to evaluate the stability of the composite membranes in the oxidizing vanadium solution.

Nuclear magnetic resonance (NMR) spectroscopy

NMR measurements were performed on a Bruker Avance 360 MHz NMR spectrometer. The following NMR experiments were performed: ^1H NMR (spectra collected at 360 MHz), ^{13}C NMR (spectra collected at 90 MHz—proton decoupled), 2-D ^1H–^1H correlation spectroscopy (COSY) and 2D ^1H–^{13}C heteronuclear multiple–quantum correlation spectroscopy (HMQC) [44,45]. The samples were prepared by dissolving approximately 50 mg of the polymer in 0.85 mL of deuterated dimethylsulfoxide (Sigma Aldrich, 99.96 atom % D); 35 μL of tetramethylsilane (TMS) was added as internal standard to all samples.

VRFB charge–discharge cycling test

VRFB experiments were carried out in an acid-resistant single cell with an active area of 25 cm^2 (Fuel Cell Technologies, Inc.). The battery was assembled by sandwiching the membrane of interest between two graphite felt electrodes (SGL Carbon, Sigracell® GFA6) previously activated by heating in an oven at 400 °C in an air atmosphere for 30 h [10]. Experiments were performed using Nafion® 212 (thickness of 50 μm) to provide a benchmark. The solutions in the negative and positive compartments (100 mL in each side) contained 1.5 M V^{2+} and VO_2^+ (sulfate salts) in 3 M H_2SO_4. Both solutions were circulated through the electrodes using two peristaltic pumps at a constant flow rate of 100 mL min^{-1}. A redox cell test system (model 857, Scribner Associates, Inc.) comprising a fluid control unit and a potentiostat with impedance spectroscopy capabilities was employed in the experiments. System control and data acquisition were done using the Flow Cell software (version 1.1, Scribner Associates, Inc.). The battery was charged and discharged at constant current densities ranging from 20 to 100 $mAcm^{-2}$ at a cell temperature of 30 °C. The flow battery was considered charged once the cell voltage reached 1.65 V and discharged when the cell voltage dropped below 0.65 V (cutoff voltages). The current efficiency (CE), energy efficiency (EE) and voltage efficiency (VE) were calculated using the following equations:

$$CE = Q_d/Q_c \times 100\% \quad (5)$$

$$EE = E_d/E_c \times 100\% \quad (6)$$

$$VE = EE/CE \times 100\% \quad (7)$$

where Q_d and Q_c were the capacity (A h) during discharging and charging of the flow battery, and E_d and E_c were the energy (W h) released during the discharge and consumed during charge, respectively.

Results and discussion

Characterization of QPEK-C/TMSP-TMA^+ composite membranes

QPEK-C AEMs were prepared through chloromethylation of PEK-C followed by quaternization using trimethylamine (TMA), with selected amounts of inorganic additive added as required to yield membranes with the desired composition (see Fig. S1 in the ESI for photographs of the pristine and composite membranes). The chemical structure of the QPEK-C-based AEMs was confirmed by ^1H NMR spectroscopy (see Fig. S2). [33]. Chloromethylation introduced 2 new protons

(chloromethyl group; $-CH_2-Cl$) that appeared at a chemical shift between 4.7 and 4.9 ppm. This peak remained almost at the same position after quaternization. A large peak corresponding to the 9 protons in the methyl groups attached to the quaternary ammonium was also found at 3.2 ppm.

Composite membranes were prepared using an *ex-situ* method by adding the appropriate amount of trimethoxysilyl propyl)-N,N,N-trimethylammonium chloride (TMSP-TMA^+, functionalized silica precursor) to QPEK-C AEM dissolved in dimethyl sulfoxide. The ion exchange capacity (IEC) and water or sulfuric acid uptake of the composite membranes of different compositions (QPEK-C/x wt%TMSP-TMA^+) were measured to investigate the relationship between these properties and ion transport properties. The IEC of the QPEK-C/x wt%TMSP-TMA^+ composite membranes increased with the loading of TMSP-TMA^+ (Table 1). We have also observed similar trends for the change in membrane water uptake and the number of water molecules per ion exchange site (λ) (Table 1 and Fig. S3). Sulfate ion conductivity increased initially with TMSP-TMA^+ loading, but for loadings above 30–40 wt%, it started to decrease (see Table 1). The concentration of quaternary ammonium groups inside the polymer matrix increased upon introduction of TMSP-TMA^+ additives, and resulted in an improvement of ion transport and hydrophilicity of the membranes. As expected, adequate hydration of quaternary ammonium moieties enhanced the ionic conductivity (see Table 1 and Fig. S3). The highest sulfate ion conductivity was 8.4 ± 0.2 mS cm^{-1} for composite membranes with 20 wt% loading of TMSP-TMA^+. Further addition of the inorganic filler resulted in a reduction of the ionic conductivity, despite further enhancement in the IEC and hydrophilicity of the membranes (i.e. increasing water uptake and λ). The reduction in ionic conductivity at relatively higher additive loadings has been frequently reported in the literature for organic/inorganic composite membranes [46–48]. Large additive loadings can lead to blockage and disruption of the ionic channels, particle agglomeration and micro-hole formation in the microstructure of the polymer matrix, all resulting in a decrease in ionic conductivity.

The addition of the functionalized inorganic additives containing cationic groups (propyl trimethylammonium) also resulted in a substantial reduction in vanadium ion permeability through the AEM. The reduction in the permeability to vanadium cations can be explained by the enhancement in the concentration of fixed cation groups, which enhance the Donnan exclusion effect. Pristine QPEK-C AEMs and QPEK-C/10-20wt%TMSP-TMA^+ composite organic/inorganic AEMs exhibited 1–2 orders of magnitude lower vanadium (IV) cation permeability when compared to Nafion® 212, which had a permeability of 3.2 × 10^{-8} cm^2s^{-1} [49].

There was no detectable VO^{2+} permeation through the composite membranes with 30 and 40 wt% TMSP-TMA^+ (see Table 1). The low permeability of the QPEK-C based AEM membranes can be explained by the following: (a) quaternary ammonium groups hinder the intrusion of the positively charged vanadium cations (Donnan effect), and (b) the relatively narrower channels in hydrocarbon based AEMs (less than 1 nm) and the larger tortuosity of the ionic channels compared to perfluorinated PEMs hinder ion transport. Furthermore, in the composite AEMs, TMSP-TMA^+ particles can partially block the ionic channels, thereby increasing the tortuosity, while the fixed groups on their surface (propyl trimethyl ammonium) allow sulfate ions to be transported (contributing to ionic conductivity), while rejecting the vanadium cations by Donnan exclusion.

The mechanical strength, flexibility and stiffness of the pristine and composite membranes were investigated by performing stress-strain measurements. The strength and flexibility of the composite membranes was modestly enhanced by incorporation of TMSP-TMA^+ up to a loading of approximately 20% (Fig. 1). However, for TMSP-TMA^+ loadings above 10–20%, both strength and flexibility started to decrease. The UTS started decreasing at loadings above 10 wt

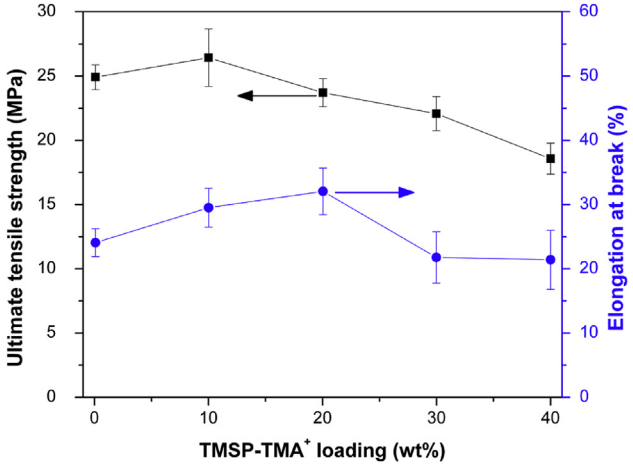

Fig. 1 – Ultimate tensile strength and elongation at break for QPEK-C AEM and QPEK-C/10-40wt%TMSP-TMA^+ composite AEMs. Tensile tests were performed at 60 °C and 50% relative humidity.

Table 1 – Ion exchange capacity, water uptake, number of water molecules per ion exchange site (λ), sulfate conductivity (σ), and VO^{2+} permeability of QPEK-C AEMs and QPEK-C/x wt%TMSP-TMA^+) organic/inorganic composite AEMs.

Membrane	IEC (meq g^{-1})	Water uptake (%)	λ	σ (mS cm^{-1})	VO^{2+} permeability (×10^{-9} cm^2 s^{-1})
QPEK-C pristine	1.11 ± 0.04	27.4 ± 1.6	13.7	4.5 ± 0.5	1.09
QPEK-C + 10 wt% TMSP-TMA^+	1.14 ± 0.03	36.5 ± 4.7	17.8	6.4 ± 0.4	0.88
QPEK-C + 20 wt% TMSP-TMA^+	1.19 ± 0.06	44.0 ± 8.9	20.5	8.4 ± 0.2	0.53
QPEK-C + 30 wt% TMSP-TMA^+	1.23 ± 0.04	51.7 ± 6.0	23.4	7.1 ± 0.5	N/A[a]
QPEK-C + 40 wt% TMSP-TMA^+	1.28 ± 0.08	69.3 ± 13.8	30.1	5.5 ± 0.6	N/A[a]

[a] No permeation of VO^{2+} was detected by UV–VIS spectroscopy after 2 weeks.

% and the EB for loadings above than 20 wt%. The lowest strength and flexibility was observed for the composite membrane with 40wt% TMSP-TMA$^+$. The stiffness of the composite membranes was estimated in terms of the Young's modulus, which was determined from the slope of the stress-strain curves in the initial linear region. The highest Young's modulus (0.11 GPa) was obtained for the pristine membranes (QPEK-C). Composite AEMs (QPEK-C/10-40wt%TMSP-TMA$^+$) were less stiff than QPEK-C AEMs and had Young's moduli in the interval 0.07–0.11 GPa. This is reasonable, assuming that the load bearing phase gradually transitions from the polymer phase to the more brittle inorganic phase with increasing additive loading.

Thermogravimetric analysis performed under nitrogen atmosphere showed that the onset temperature for degradation of QPEK-C/10-40wt%TMSP-TMA$^+$ composite membranes was approximately 20 °C higher than for QPEK-C AEM (see Figs. S4–S6 in the ESI).

Stability test of QPEK-C/TMSP-TMA$^+$ composite membranes in VO_2^+ oxidizing solution

A membrane separator should have adequate ionic conductivity and mechanical properties, but, most importantly, it should maintain its properties thousands of charge–discharge cycles (and hence thousands of hours). It is well-known that the degradation of aromatic polymer backbones results from the oxidative attack by VO_2^+ [27]. To investigate the chemical stability of QPEK-C/TMSP-TMA$^+$ composite AEMs under the highly oxidizing conditions found in an operating VRFB, we immersed the membranes in 1.5 M VO_2^+ solution in 3 M sulfuric acid, and monitored the changes in sulfate ion conductivity, UTS and EB over about 700 h. In our previous study [33], QPEK-C AEMs (pristine membranes, without addition of any inorganic fillers) maintained their initial ionic conductivity after 1400 h in 1.5 M VO_2^+ + 3 M H_2SO_4. However, in this study, we must report that the QPEK-C/TMSP-TMA$^+$ composite AEMs degrade relatively fast under the same test conditions. Fig. 2 shows the change of sulfate ion conductivity for QPEK-C AEM and composite AEMs with 10, 20, 30, and 40 wt% of TMSP-TMA$^+$, after immersion in 1.5 M VO_2^+ + 3 M H_2SO_4. The initial decrease in sulfate ion conductivity (approximately 1 mS cm^{-1}) observed for QPEK-C AEMs (pristine) was attributed to the intrusion of vanadium cations into the ionic channels of the polymer matrix [33]. However, the ionic conductivity of the composite membranes decreased considerably after 72 h exposure to the VO_2^+ solution. We hypothesize that the decrease in the ionic conductivity was due to the oxidation of TMSP-TMA$^+$ additives by the presence of VO_2^+ (a relatively strong oxidant species). Fig. S7 and the accompanying text in the ESI provide some evidence to support this hypothesis.

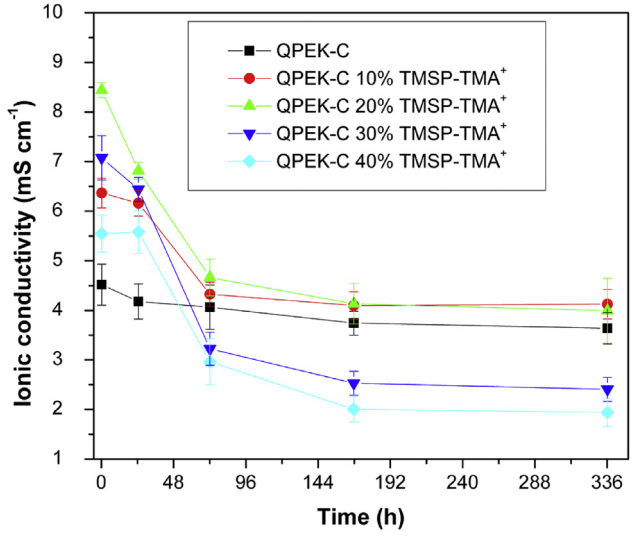

Fig. 2 – The effect of exposure to 1.5 M VO_2^+ + 3 M H_2SO_4 (at 30 °C) on sulfate ionic conductivity of QPEK-C and QPEK-C/10-40wt%TMSP-TMA$^+$ composite AEMs.

After 360 h immersed in 1.5 M VO_2^+ + 3 M H_2SO_4, the sulfate ion conductivity of QPEK-C/10&20wt%TMSP-TMA$^+$ composite AEMs dropped to the same value of the ionic conductivity of the pristine membrane, while the ionic conductivity of QPEK-C/30&40wt%TMSP-TMA$^+$ dropped to much lower values (see Fig. 2). The change in the chemical structure of TMSP-TMA$^+$ was investigated by performing two-dimensional NMR spectroscopy (^{1}H–^{1}H homonuclear correlation spectroscopy, COSY; and ^{1}H–^{13}C heteronuclear single quantum correlation spectroscopy, HMQC). The degradation of TMSP-TMA$^+$ after immersion in 1.5 M VO_2^+ + 3 M H_2SO_4 was revealed by using COSY spectroscopy (Fig. S7). The detachment of trimethylammonium functional groups after 72 h exposure to the VO_2^+ solution was confirmed by the absence of the proton–proton couplings between the adjacent protons in the propyl linking group, initially present at chemical shifts of 3.1 ppm and 3.4 ppm. After immersion in the vanadium solution, a new peak in the ^{1}H NMR spectrum was observed at 5.28 ppm; however, the same peak was not observed in the ^{1}H–^{13}C HMQC spectrum, demonstrating that the protons were directly bonded to carbon. The new peak was attributed to a hydroxide group that could result from the oxidation of TMSP-TMA$^+$ by VO_2^+ and/or H_2SO_4. Thus, under strong oxidizing conditions (VO_2^+ + H_2SO_4), TMSP-TMA$^+$ degrades and this results in the removal of the active functional groups. However, we note that the reduction in vanadium ion permeability by physical blockage of the ion transport pathways was still effective in the degraded additives.

The mechanical properties and the stability under oxidizing conditions, of QPEK-C and composite AEMs, were investigated by monitoring UTS, EB, and Young's modulus (see Figs. S8–S10 in the ESI). Changes in the UTS are a good indicator of change in the polymer molecular weight [33]. However, during the stability tests, we did not observe any changes in the UTS of the AEMs. These results demonstrated that the polymer backbone remained stable upon immersion in 1.5 M VO_2^+. But, the EB (for all the AEMs) decreased within a week of exposure to the oxidizing solution. We attribute this observation to the intrusion of immovable vanadium cations into the polymer matrix. As a consequence of the vanadium cation intrusion, the composite membranes became more stiff. Even though TMSP-TMA$^+$ additives were not chemically stable when immersed in the oxidizing VO_2^+ solution, the degradation of the additives did not significantly influence the mechanical properties of QPEK-C/TMSP-TMA$^+$ AEM composites.

Single-cell VRFB charge–discharge cycling tests

Fig. 3 shows the CEs and EEs of VRFBs (operated at constant current densities ranging from 20 to 100 $mAcm^{-2}$) assembled with QPEK-C AEM, QPEK-C/20wt%TMSP-TMA^+ composite AEM, and Nafion® 212 PEM membrane separators. When the current density was increased, it took less time for a full charge or discharge in the VRFBs, which resulted in higher CEs. The retention time for a single charge–discharge cycle is a dominant factor that determines the CE in a VRFB system [34]. Longer times to charge and discharge the battery leads to more cation (vanadium) cross-mixing via transport through the membrane separator. Composite AEMs (QPEK-C/10-40 wt% TMSP-TMA^+) had lower VO^{2+} permeability than QPEK-C (see Table 1), resulting typically in a higher CE than when using Nafion® 112 as separator. However, in this study, we found that the differences between CEs for Nafion® and for the composite membranes were only significant when the flow battery was charged and discharged at current densities below 60 mA cm^{-2}. In Fig. S13, we show a typical voltage vs. time charge/discharge curve for a vanadium redox flow battery assembled with a QPEK-C +20wt%TMSP-TMA^+ AEM separator. The battery was operated at a current density of 100 $mAcm^{-2}$. For current densities in the interval 60–100 mA cm^{-2}, the CEs for Nafion® 212, QPEK-C and QPEK-C/20wt% TMSP-TMA^+ were very close (even though Nafion® 112 had a relatively higher VO^{2+} permeability). At a current density of 100 mA cm^{-2}, QPEK-C AEMs and QPEK-C/20wt% TMSP-TMA^+ composite AEMs resulted in CEs of 99% and 96%, respectively.

The cell resistance was measured continuously during the flow battery experiments. The frequency response analyzer (FRA) built-in the redox flow battery station was set at a frequency of 5000 Hz to obtain the high frequency resistance (HFR), which is directly related to the area-specific resistance (ASR) of the cell. The ASR (at 100 $mAcm^{-2}$) for Nafion® 212, QPEK-C and QPEK-C^+ 20wt% TMSP-TMA^+ were 1000 ± 25 mOhm cm^2, 2150 ± 100 mOhm cm^2 and 1150 ± 50 mOhm cm^2, respectively.

EE (product of VE by CE) is governed dominantly by the VE because the CE is close to 100%. Even if the membrane has some effect on CE due to cation intermixing, the typical current densities used to charge and discharge the flow battery make the differences too small, and hence the differences in CEs can be neglected. Both VE and EE decreased monotonically as the current density increased from 20 to 100 mA cm^{-2} (see Fig. 3 and Fig. S11). The reduction in VE resulted from an increase in cell overpotentials with increasing current density. QPEK-C/20wt% TMSP-TMA^+ composite AEMs exhibited larger EEs than QPEK-C AEMs (pristine) because of the lower ohmic resistance of the membrane. The EEs and VEs of the VRFBs employing QPEK-C AEM, QPEK-C/20wt% TMSP-TMA^+ composite AEM, and Nafion® 212 were in good agreement with the polarization curves obtained for a battery state of charge (SoC) of 50% (See Fig. S12 in the ESI). At a SoC of 100% and a current density of 100 mA cm^{-2}, comparable cell voltages of 1.44, 1.48, and 1.47 V were achieved for VRFBs employing Nafion® 212, QPEK-C AEM and QPEK-C/20wt% TMSP-TMA^+ composite AEM, respectively.

The electrochemical activity of the electrodes towards change/discharge reactions, the ohmic resistance of the membrane, and capacity fading are critical factors that determine VRFB performance during long-term operation. We have assumed that the kinetics at the electrodes were the same for the VRFBs employing Nafion®, QPEK-C and QPEK-C/20wt% TMSP-TMA^+ composite AEMs as identical carbon felt electrodes and activation processes were used in all the experiments.

The transport of active vanadium species through the membrane separator during battery charge/discharge resulted in capacity fading. Capacity fading was relatively high for Nafion® 212 separator when compared with the AEM separators (Fig. 4). After 30 charge–discharge cycles (approximately 60 h), battery capacity faded approximately by 30% when using Nafion® 212 separator, while only 10% capacity loss was

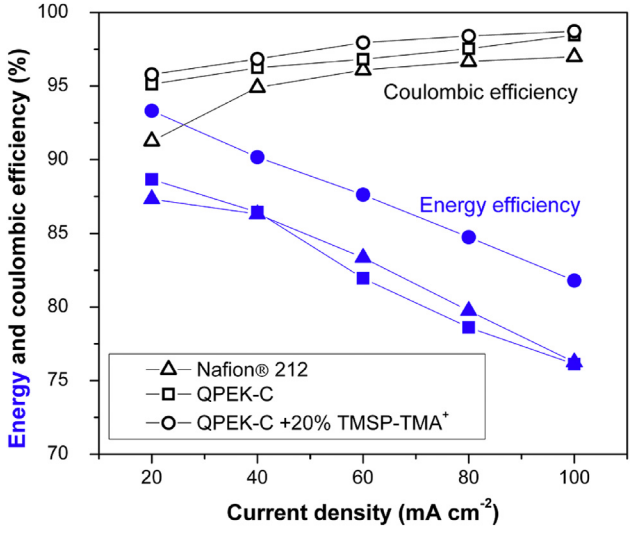

Fig. 3 – Energy and coulombic efficiencies for VRFBs employing Nafion® 212, QPEK-C, or QPEK-C/20 wt% TMSP-TMA^+ as membrane separators.

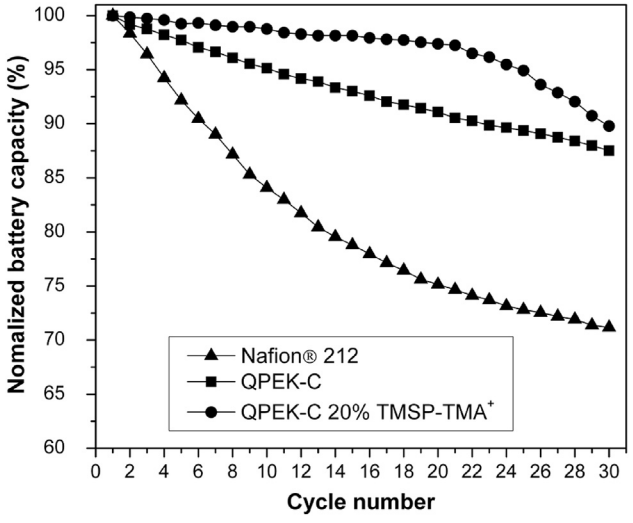

Fig. 4 – Capacity fading for VRFBs employing Nafion® 212, QPEK-C, or QPEK-C/20 wt% TMSP-TMA^+ as membrane separators.

observed with QPEK-C AEM and QPEK-C/20wt% TMSP-TMA$^+$ composite AEMs.

Capacity fading degrades the EE during long-term testing, as shown in Fig. 5. The average voltage dropped with the number of cycles due to the decrease in flow battery capacity, and resulted in lower VE and EEs. Over 30 charge–discharge cycles, about 8% loss in EE was observed in a VRFB employing QPEK-C/20wt% TMSP-TMA$^+$ composite AEM, while only 3–4% loss in the EE was observed in a VRFBs employing Nafion® 212 and QPEK-C AEM. There are several reasons to explain the decrease of EEs over longer operational times. One reason is loss of electrode activity. However, since we had used the same electrodes for all the cells, this can not explain the differences encountered between the membranes tested. We can also attribute the more rapid degradation of EE in VRFBs using composite AEM separators membranes to the degradation of the TMSP-TMA$^+$ inorganic additive during battery operation. Despite the degradation of the inorganic additives in the composite membrane, the final EEs obtained using these separators (after 30 charge–discharge cycles) were slightly higher than VRFBs assembled with QPEK-C AEM and Nafion® 212. The CEs in VRFBs employing QPEK-C AEM (pristine) and QPEK-C/20wt% TMSP-TMA$^+$ composite AEMs were retained at approximately 99% over 30 charging/discharging cycles. The CE when using Nafion® 212 separator was about 95–96% over this timeframe.

Conclusions

Quaternized cardo-poly(etherketone) (QPEK-C) AEMs and organic/inorganic composite AEMs containing QPEK-C and 10-40 wt% of N-(trimethoxysilylpropyl)-N,N,N-trimethylammonium chloride (TMSP-TMA$^+$Cl$^-$) were synthesized, characte rized and evaluated as separators for all-vanadium redox flow batteries (VRFB). As the loading of TMSP-TMA$^+$ was increased from 0 to 20wt%, the ion exchange capacity (IEC), water uptake, and number of water molecules per ion exchange site increased monotonically from 1.11 ± 0.04 meq g^{-1}, 27.4 ± 1.6wt %, and 14 to 1.28 ± 0.08 meq g^{-1}, 69.3 ± 13.8wt%, and 30, respectively. Composite membranes with 20 wt% of TMSP-TMA$^+$ (QPEK-C/20wt%TMSP-TMA$^+$) exhibited a maximum in ionic (sulfate ion) conductivity, and half of the VO^{2+} permeability of the pristine QPEK-C AEM. The VO^{2+} permeability through QPEK-C/30wt%TMSP-TMA$^+$ and QPEK-C/40wt% TMSP-TMA$^+$was extremely low, and it was not possible to detect any ion permeability for up to 2 weeks. The UTS and EB (% of initial length) displayed a maximum for the QPEK-C/10-20wt%TMSP-TMA$^+$ composite AEMs (26 ± 2 MPa and 32 ± 3%). Further increase of TMSP-TMA$^+$ loading resulted in a decrease of UTS and EB.

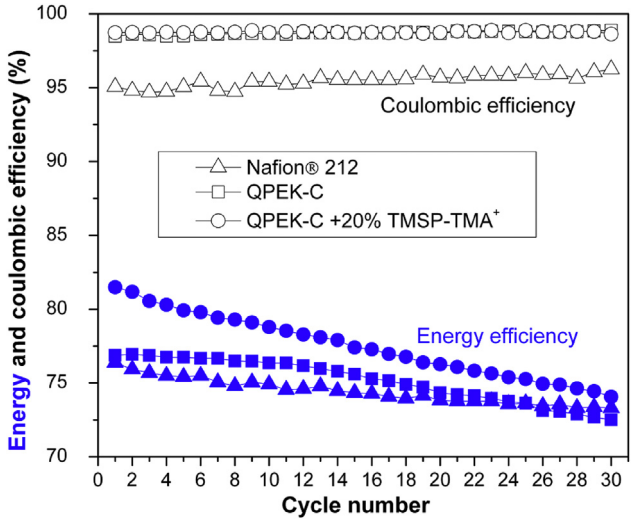

Fig. 5 – Energy and coulombic efficiencies for VRFBs empoying Nafion® 212, QPEK-C AEM, and QPEK-C/20 wt% TMSP-TMA$^+$ as membrane separators. The charging/discharging tests were done during 30 cycles at a current density of 100 mAcm^{-2}.

The chemical stability of the AEMs and TMSP-TMA$^+$ additives were investigated by immersing QPEK-C/TMSP-TMA$^+$ composite AEMs and a TMSP-TMA$^+$ powder in a 1.5 M VO_2^+ + 3 M H_2SO_4 oxidizing solution at 30 °C. After 72 h, we observed a drop of the ionic conductivity (sulfate form) of the composite AEMs. However, the composite AEMs remained mechanically stable. 1-D (^{1}H) and 2-D NMR spectroscopy (COSY) also confirmed the oxidative degradation of TMSP-TMA$^+$ filler. QPEK-C was found to be stable in VO_2^+ solutions for over 2 weeks.

Nafion® 212, QPEK-C AEM, and QPEK-C/20wt%TMSP-TMA$^+$ composite AEM were employed as separators in a VRFB operated at the following current densities: 20, 40, 60, 80, and 100 mA cm^{-2}. VRBs operated with a QPEK-C/20wt%TMSP-TMA$^+$ composite AEM yielded an energy efficiency (EE) 6% higher that QPEK-C AEM and Nafion® 212 membrane. Approximately 10% capacity fade during 30 charging/discharging cycles (approximately 60 h), was observed when using QPEK-C AEM and QPEK-C/20wt%TMSP-TMA$^+$ composite AEM as the membrane separator in a VRFB. 30% capacity fade was measured for a Nafion® 212 membrane separator. The EE of QPEK-C/20wt%TMSP-TMA$^+$ composite AEM was in the interval 74–82% (during the 30 charging/discharging cycles), while Nafion® 212 and the QPEK-C AEM provided relatively constant EEs in the range 72–76%.

In conclusion, QPEK-C and QPEK-C/TMSP-TMA$^+$ composite AEMs can effectively delay efficiently vanadium species cross-mixing, resulting in reasonable CE and EE. Despite TMSP-TMA$^+$ degradation in VO_2^+ solutions, the EEs in VRFB employing QPEK-C/20wt%TMSP-TMA$^+$ were higher than for QPEK-C AEM and Nafion® 212 membrane separators. The improvements in ionic conductivity achieved by introducing TMSP-TMA$^+$ functionalized inorganic filler into the QPEK-C polymeric matrix were substantial (providing ample proof of concept for our proposed approach), however, due to the degradation of TMSP-TMA$^+$ in presence of VO_2^+, it is necessary to develop more stable functionalized inorganic materials.

Acknowledgments

V.R. acknowledges the Office of Naval Research (contract number N00014-14-1-0705) for funding work related to anion exchange membranes and the S. R. Cho Endowed Chair Professorship for funding the flow battery work. We would also

like to acknowledge the Research Resource Center at the University of Illinois at Chicago and Dr. Robert Kleps for access to the 360 MHz Bruker NMR instrument used during this work.

Appendix A. Supplementary data

Supplementary data related to this article can be found at http://dx.doi.org/10.1016/j.ijhydene.2016.04.060.

REFERENCES

[1] Kear G, Shah AA, Walsh FC. Development of the all-vanadium redox flow battery for energy storage: a review of technological, financial and policy aspects. Int J Energy Res 2012;36:1105–20.
[2] Dunn B, Kamath H, Tarascon J-M. Electrical energy storage for the grid: a battery of choices. Science 2011;334:928–35.
[3] Mohammadi T, Kazacos MS. Evaluation of the chemical stability of some membranes in vanadium solution. J Appl Electrochem 1997;27:153–60.
[4] Prifti H, Parasuraman A, Winardi S, Lim TM, Skyllas-Kazacos M. Membranes for redox flow battery applications. Membranes 2012;2:275–306.
[5] Rychcik M, Skyllas-Kazacos M. Characteristics of a new all-vanadium redox flow battery. J Power Sources 1988;22:59–67.
[6] Skyllas-Kazacos M, Chakrabarti MH, Hajimolana SA, Mjalli FS, Saleem M. Progress in flow battery research and development. J Electrochem Soc 2011;158:R55–79.
[7] Skyllas-Kazacos M, Kasherman D, Hong DR, Kazacos M. Characteristics and performance of 1 kW UNSW vanadium redox battery. J Power Sources 1991;35:399–404.
[8] Skyllas-Kazacos M, Rychcik M, Robins RG, Fane AG, Green MA. New all-vanadium redox flow cell. J Electrochem Soc 1986;133:1057–8.
[9] Sum E, Skyllas-Kazacos M. A study of the vanadium(II)/vanadium(III) redox couple for redox flow cell applications. J Power Sources 1985;15:179–90.
[10] Sun B, Skyllas-Kazacos M. Modification of graphite electrode materials for vanadium redox flow battery application. I. Thermal treatment. Electrochim Acta 1992;37:1253–60.
[11] Wang W, Kim S, Chen B, Nie Z, Zhang J, Xia G-G, et al. A new redox flow battery using Fe/V redox couples in chloride supporting electrolyte. Energy Environ Sci 2011;4:4068–73.
[12] Yu EH, Wang X, Krewer U, Li L, Scott K. Direct oxidation alkaline fuel cells: from materials to systems. Energy Environ Sci 2012;5:5668–80.
[13] Li X, Zhang H, Mai Z, Zhang H, Vankelecom I. Ion exchange membranes for vanadium redox flow battery (VRB) applications. Energy Environ Sci 2011;4:1147–60.
[14] Mauritz KA, Moore RB. State of understanding of Nafion. Chem Rev 2004;104:4535–85.
[15] Le XT. Contribution to the study of properties of Selemion AMV anion exchange membranes in acidic media. Electrochim Acta 2013;108:232–40.
[16] Kolde JA, Bahar B, Wilson MS, Zawodzinski TA, Gottesfeld S. Advanced composite polymer electrolyte fuel cell membranes. Proc - Electrochem Soc 1995;95–23:193–201.
[17] Sata T. Properties of composite membranes formed from ion-exchange membranes and conducting polymers. 4. Change in membrane resistance during electrodialysis in the presence of surface-active agents. J Phys Chem 1993;97:6920–3.
[18] Palaty Z, Zakova A, Dolecek P. Modelling the transport of Cl^- ions through the anion-exchange membrane NEOSEPTA-AFN Systems HCl/membrane/H_2O and HCl-$FeCl_3$/membrane/H_2O. J Membr Sci 2000;165:237–49.
[19] Schreiber M, Harrer M, Whitehead A, Bucsich H, Dragschitz M, Seifert E, et al. Practical and commercial issues in the design and manufacture of vanadium flow batteries. J Power Sources 2012;206:483–9.
[20] Chen D, Kim S, Li L, Yang G, Hickner MA. Stable fluorinated sulfonated poly(arylene ether) membranes for vanadium redox flow batteries. RSC Adv 2012;2:8087–94.
[21] Kalappa P, Lee J-H. Proton conducting membranes based on sulfonated poly(ether ether ketone)/TiO_2 nanocomposites for a direct methanol fuel cell. Polym Int 2007;56:371–5.
[22] Kim S, Yan J, Schwenzer B, Zhang J, Li L, Liu J, et al. Cycling performance and efficiency of sulfonated poly(sulfone) membranes in vanadium redox flow batteries. Electrochem Commun 2010;12:1650–3.
[23] Kreuer KD. On the development of proton conducting polymer membranes for hydrogen and methanol fuel cells. J Membr Sci 2001;185:29–39.
[24] Li X, Yu Y, Meng Y. Novel quaternized poly(arylene ether sulfone)/nano-ZrO_2 composite anion exchange membranes for alkaline fuel cells. ACS Appl Mater Interfaces 2013;5:1414–22.
[25] Mai Z, Zhang H, Li X, Bi C, Dai H. Sulfonated poly(tetramethydiphenyl ether ether ketone) membranes for vanadium redox flow battery application. J Power Sources 2011;196:482–7.
[26] Cumbal L, SenGupta AK. Arsenic removal using polymer-supported hydrated iron(III) oxide nanoparticles: role of Donnan membrane effect. Environ Sci Technol 2005;39:6508–15.
[27] Chen D, Hickner MA. V5+ degradation of sulfonated Radel membranes for vanadium redox flow batteries. Phys Chem Chem Phys 2013;15:11299–305.
[28] Xi J, Li Z, Wu Z, Qiu X. Manufacturing of sulfonated polyether ether ketone-based blend ion-exchange membrane for redox flow battery. Peop. Rep. China: Graduate School at Shenzhen, Tsinghua University; 2013. p. 11.
[29] Zhang Q, Dong Q-F, Zheng M-S, Tian Z-W. The preparation of a novel anion-exchange membrane and its application in all-vanadium redox batteries. J Membr Sci 2012;421–422:232–7.
[30] M-sJ Jung, Parrondo J, Arges CG, Ramani V. Polysulfone-based anion exchange membranes demonstrate excellent chemical stability and performance for the all-vanadium redox flow battery. J Mater Chem A 2013;1:10458–64.
[31] Zhang S, Yin C, Xing D, Yang D, Jian X. Preparation of chloromethylated/quaternized poly(phthalazinone ether ketone) anion exchange membrane materials for vanadium redox flow battery applications. J Membr Sci 2010;363:243–9.
[32] Zhang B, Zhang S, Xing D, Han R, Yin C, Jian X. Quaternized poly(phthalazinone ether ketone ketone) anion exchange membrane with low permeability of vanadium ions for vanadium redox flow battery application. J Power Sources 2012;217:296–302.
[33] Yun S, Parrondo J, Ramani V. Derivatized cardo-polyetherketone anion exchange membranes for all-vanadium redox flow batteries. J Mater Chem A 2014;2:6605–15.
[34] Fang J, Xu H, Wei X, Guo M, Lu X, Lan C, et al. Preparation and characterization of quaternized poly (2,2,2-trifluoroethyl methacrylate-co-N-vinylimidazole) membrane for vanadium redox flow battery. Polym Adv Technol 2013;24:168–73.
[35] Nagarale RK, Gohil GS, Shahi VK, Rangarajan R. Preparation of organic-inorganic composite anion-exchange membranes

via aqueous dispersion polymerization and their characterization. J Colloid Interface Sci 2005;287:198–206.
[36] Schwenzer B, Zhang J, Kim S, Li L, Liu J, Yang Z. Membrane development for vanadium redox flow batteries. ChemSusChem 2011;4:1388–406.
[37] Kumar M, Singh S, Shahi VK. Cross-linked poly(vinyl alcohol)-poly(acrylonitrile-co-2-dimethylamino ethylmethacrylate) based anion-exchange membranes in aqueous media. J Phys Chem B 2010;114:198–206.
[38] Takimoto N, Takamuku S, Abe M, Ohira A, Lee H-S, McGrath JE. Conductive area ratio of multiblock copolymer electrolyte membranes evaluated by e-AFM and its impact on fuel cell performance. J Power Sources 2009;194:662–7.
[39] Jiang R, Kunz HR, Fenton JM. Composite silica/Nafion membranes prepared by tetraethylorthosilicate sol-gel reaction and solution casting for direct methanol fuel cells. J Membr Sci 2006;272:116–24.
[40] Wu Z, Sun G, Jin W, Hou H, Wang S, Xin Q. Nafion and nano-size $TiO_2SO_4^{2-}$ solid superacid composite membrane for direct methanol fuel cell. J Membr Sci 2008;313:336–43.
[41] Sambandam S, Ramani V. SPEEK functionalized silica composite membranes for polymer electrolyte fuel cells. Prepr Symp - Am Chem Soc Div Fuel Chem 2007;52:323–4.
[42] Singh S, Jasti A, Kumar M, Shahi VK. A green method for the preparation of highly stable organic inorganic hybrid anion-exchange membranes in aqueous media for electrochemical processes. Polym Chem 2010;1:1302–12.
[43] Wei X, Nie Z, Luo Q, Li B, Chen B, Simmons K, et al. Nanoporous Polytetrafluoroethylene/silica composite separator as a high-performance all-vanadium redox flow battery membrane. Adv Energy Mater 2013;3:1215–20.
[44] Arges CG, Ramani V. Two-dimensional NMR spectroscopy reveals cation-triggered backbone degradation in polysulfone-based anion exchange membranes. Proc Natl Acad Sci U S A 2013;110:2490–5.
[45] Arges CG, Ramani V. Investigation of cation degradation in anion exchange membranes using multi-dimensional NMR spectroscopy. J Electrochem Soc 2013;160:F1006–21.
[46] Xu T, Hou W, Shen X, Wu H, Li X, Wang J, et al. Sulfonated titania submicrospheres-doped sulfonated poly(ether ether ketone) hybrid membranes with enhanced proton conductivity and reduced methanol permeability. J Power Sources 2011;196:4934–42.
[47] Nagarale RK, Shin W, Singh PK. Progress in ionic organic-inorganic composite membranes for fuel cell applications. Polym Chem 2010;1:388–408.
[48] Kim DJ, Hwang HY, Nam SY, Hong YT. Characterization of a composite membrane based on SPAES/sulfonated montmorillonite for DMFC application. Macromol Res 2012;20:21–9.
[49] Chen D, Hickner MA, Agar E, Kumbur EC. Optimized anion exchange membranes for vanadium redox flow batteries. ACS Appl Mater Interfaces 2013;5:7559–66.